Conference on Modelling Fluid Flow (CMFF'22)
The 18th International Conference on Fluid Flow Technologies
Budapest, Hungary, August 30 -September 2, 2022

EFFECTS OF TIP LEAKAGE VORTEX CAVITATION ON FLOW FIELD UNDER CAVITATION INSTABILITY

Youngkuk YOON[1], Seung Jin SONG[2]

[1] Department of Mechanical Engineering, Seoul National University. 1 Gwanak-ro, Gwanak-gu, Seoul, Korea. Tel.: +82 2 880 1701, E-mail: truesky1218@snu.ac.kr
[2] Corresponding Author, Department of Mechanical Engineering, Seoul National University. 1 Gwanak-ro, Gwanak-gu, Seoul, Korea. Tel.: +82 2 880 1667, E-mail: sjsong@snu.ac.kr

ABSTRACT

Cavitation instabilities induce axial and circumferential vibration, and noise in turbopump inducers. Therefore, the purpose of the present study is to investigate the mechanism of the cavitation instability. Flow field near the two-bladed inducer leading edge under alternate blade cavitation was experimentally investigated by using particle image velocimetry (PIV). It was found that the tip leakage vortex cavitation draws the flow toward its region of collapse and induce negative angle of attack change to the adjacent blade. Also, this cavity-blade interaction was shown to be the main cause of the alternate blade cavitation. It was further shown that this cavity-blade interaction is the strongest when the cavity collapse occurs in the inducer throat area under which the pressure perturbation due to alternate blade cavitation is the largest.

Keywords : cavitation instability, inducer, PIV

NOMENCLATURE

c*	[m]	inducer throat chordwise length
α	[DEG]	incidence angle
$\Delta\alpha$	[DEG]	change in incidence angle
σ	[-]	cavitation number
ϕ	[-]	flow coefficient

1. INTRODUCTION

Inducer cavitation instabilities cause serious noise and vibration which can lead to a failure of propulsion system. Therefore, their types and identification have gained much attention. For example, Tsujimoto et al. [1] observed various cavitation instabilities which occurred in three-bladed inducer and categorized them into local instabilities such as super-synchronous rotating cavitation and global instabilities such as cavitation surge. Also, Cervone et al. [2] experimentally observed a cavitation instability called alternate blade cavitation with two-bladed inducer. These various cavitation instabilities have different frequency and spatial mode characteristics which can be identified via Fourier transformation and circumferential unsteady pressure measurements.

To predict the cavitation instability and to analyse its mechanism, various models have been suggested. Tsujimoto et al. [3] used an actuator disk method to predict rotating cavitation. In the method, quasi-steady lumped parameters such as mass flow gain factor and cavitation compliance are introduced, and it was shown that the mass flow gain factor plays a key role in the cavitation instability. Also, Watanabe et al. [4] and Horiguchi et al. [5] performed stability analysis using singularity method. They predicted various cavitation instabilities including forward and backward propagating rotating cavitation. However, the above methods cannot adequately reflect the 3-D nature of the inducer cavitation, which is mostly composed of tip leakage vortex cavitation (TLVC). Therefore, 3-D numerical approach and experiments have been conducted to investigate the cavitation instability mechanism. Kang et al. [6] conducted 3-D numerical simulation and showed that cavitation instabilities begin to occur when the cavity on a blade interacts with the adjacent blade leading edge. Kim and Song [7] performed an experimental investigation on rotating cavitation and showed that the cavitation decreases the incidence angle of the following blade via particle image velocimetry (PIV) and high-speed visualization. However, even though these studies proposed the mechanism of cavity-blade interaction for the cavitation instability, only few selected cases have been examined in the research.

Therefore, in the present research, the interaction between cavity and the flow field is investigated under various operating condition for two-bladed inducer. PIV was used to quantify the change in velocity field around blade leading edge

and, furthermore, the cavity-blade interaction under alternate blade cavitation.

2. EXPERIMENTAL SETUP

Experiments have been performed with Seoul National University Water Tunnel (SNUWT, Figure 1). SNUWT is composed of a water tank, electric heater, flow meter, booster pump, control valve, and an inducer test section to control flow coefficient and cavitation number independently. Also, a filtration chamber prevents the particle with size larger than 1 micron from entering the test facility. A detailed description of the facility is given in Kim and Song [7].

To determine the cavitation number and to identify cavitation instability, steady and unsteady pressure measurement were conducted. Four pneumatic pressure sensors (Druck PMP 5073) were mounted at inlet and outlet of the inducer, and five unsteady pressure transducers (Kulite HKM-375) were flush-mounted at the inducer inlet casing. Also, for PIV, inducer casing was made of transparent acryl. Litron L 200-15 PIV laser and Phantom v2640 camera were used for the flow field measurement.

A Two-bladed inducer was examined in the present research (Figure 2). Details about the inducer can be found in [8]. All the experiments were conducted under design flow coefficient, and the cavitation number was lowered from non-cavitating condition to near super-cavitating condition which showed severe alternate blade cavitation.

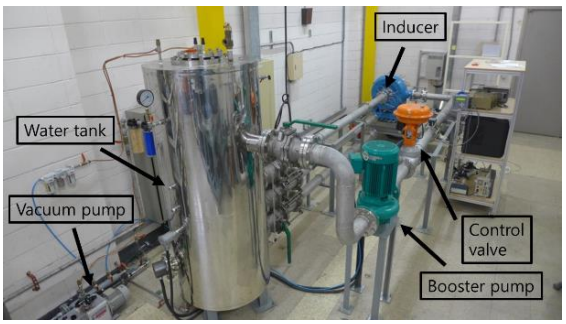

Figure 1. Seoul National University Water Tunnel

3. EXPERIMENT RESULTS AND DISCUSSION

To quantify the blade-cavity interaction, firstly, the flow field near blade leading edge under non-cavitating condition was obtained and averaged over region of interest as shown in Figure 3.

The background image of the Fig. 3 is the raw image under continuous lighting filmed with high-speed camera. Also, the overlapped particle images are taken under pulsed laser lighting and the green vectors are resulting velocity vectors. The red dotted box shows the area over which the velocity vectors are averaged to determine the mean velocity vector near blade leading edge.

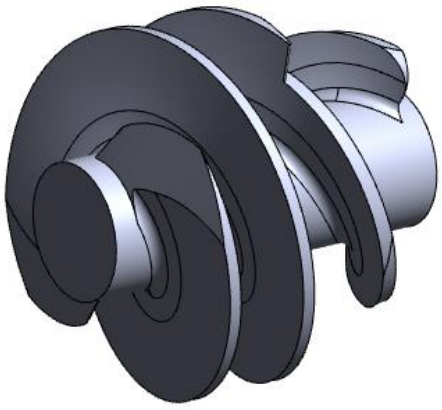

Figure 2. Geometry of the test inducer

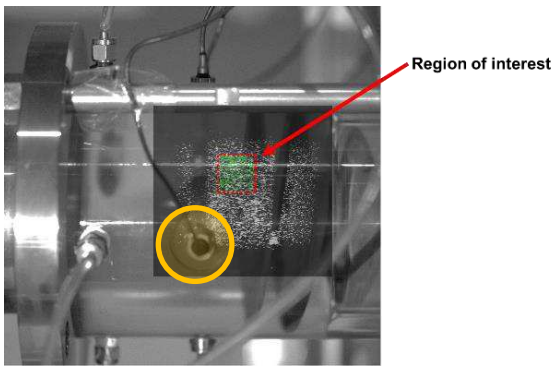

Figure 3. PIV region of interest

Then, at cavitating condition, the same calculation is proceeded and the difference between mean velocity vectors is obtained. Under alternate blade cavitation, leading edges of the two blades are treated separately due to asymmetry of cavity. Finally, these velocity differences are converted to change in angle of attack in rotating frame ($\Delta\alpha$). In the present study, $\Delta\alpha$ was used to represent the cavity-blade interaction.

In the present study, the occurence of the alternate blade cavitation is examined via unsteady pressure measurement at the inducer casing inlet. At 0.15D, where D is the inducer casing diameter, upstream of the inducer tip leading edge, unsteady pressure transducer is flush-mounted, which is highlighted as an orange circle in Fig. 3, and sampled at 2,000 sampes per second. During experiment, inlet pressure, and therefore, cavitation number is decreased. While decreasing the cavitation number, the unsteady pressure signal, whose DC component is filetered, is Fourier-transformed to examine the alternate blade cavitation. Figures 4 and 5 show the typical Fourier transformation results under equal-length cavitation (symmetrical development of the cavitation without cavitaiton instability) and alternate blade caviation. In both cases, peak is observed at normalized frequency of 2, due to the

blade passing frequency of the two-bladed inducer. If the system is under alternate blade cavitation as shown in Fig. 5, normalized frequency of 1 (which equals the shaft rotating frequency) is excited due to the asymmetry of the alternate blade cavitation. Figure 6 visualizes the asymmetry of cavity development under alternate blade cavitation. Both long and short cavities are developed on different blades, and this asymmetric pattern is attached to the blade and remains stationary in the rotating frame. Therefore, not only the blade passing frequency, the shaft rotating frequency is also strongly excited. This peak at normalized frequency of 1 is used to judge whether the alternate bladce cavitaiton occurs and its magnitude can be used to represent the strength of the instability. In the experiment, the magnitude of the Fourier coefficient and the difference between two cavity lengths show the same trend, and thus they were both used to represent the magnitude of the alternate blade cavitation.

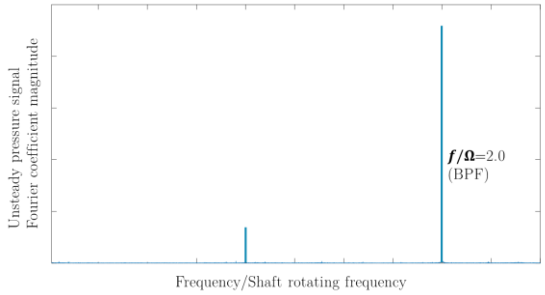

Figure 4. Typical frequency traces under equal-length cavitation

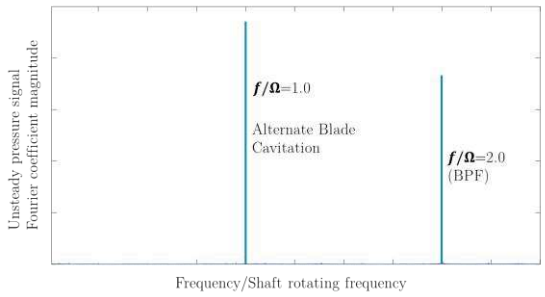

Figure 5. Typical frequency traces under two-bladed inducer alternate blade cavitation

Due to the strong axial flow induced by the collapsing cavity, Δα has negative sign in most of the situation. Figures 7, 8, and 9 shows the flow field vector plot at the PIV region of interest under non-cavitating condition and alternate blade cavitation. In Figs. 8 and 9, both blades 1 & 2 are shown to compare the effect of the larger cavity and the smaller cavity. In Fig. 7, it can be seen that the backflow is developed near the blade leading edge due to adverse pressure gradient of the inducer. In Fig. 8, similar flow structure is developed near the blade 1 leading edge (blades are numbered as 1 and 2, corresponding the blade with larger cavity and smaller cavity under alternate blade cavitation, respectively). Therefore, the smaller cavity induced at blade 2 is not enough developed to interact with the leading edge of the following blade.

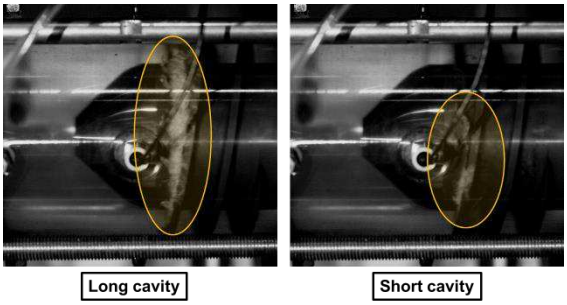

Figure 6. Visualization of alternate blade cavitation

However, as can be seen in Fig. 9, strong axial flow is developed at the blade 2 leading edge. This is due to cavity collapse near the blade 2 leading edge. While the cavity developed at blade 1 is large enough to interact with the following blade leading edge, it collapses due to high pressure downstream and drags the surrounding fluid to create strong axial flow. This axial flow decreases the incidence of the following blade and inhibits the cavity development.

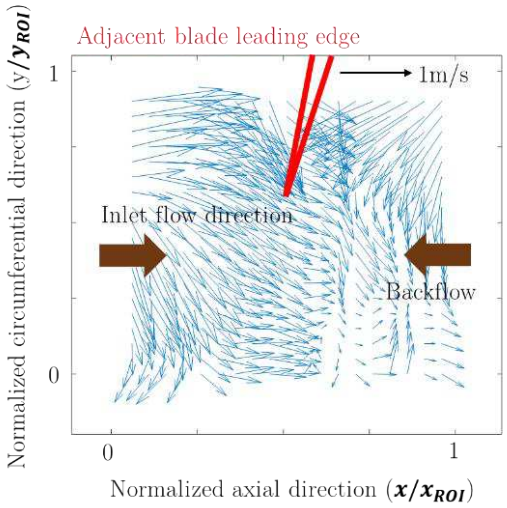

Figure 7. Flow field near blade leading edge at non-cavitating condition

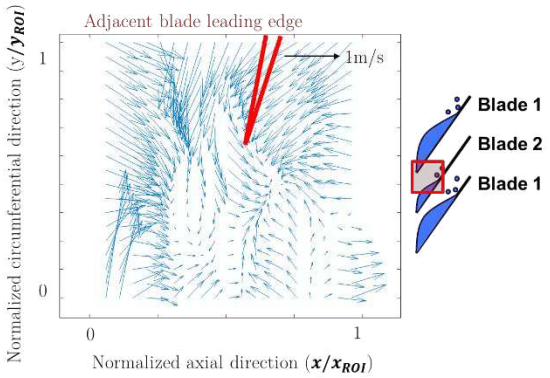

Figure 8. Flow field near blade 1 leading edge under alternate blade cavitation

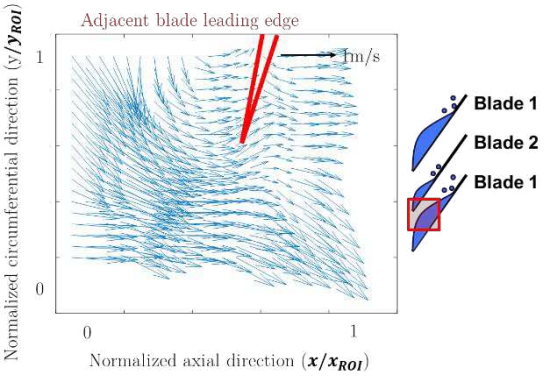

Figure 9. Flow field near blade 2 leading edge under alternate blade cavitation

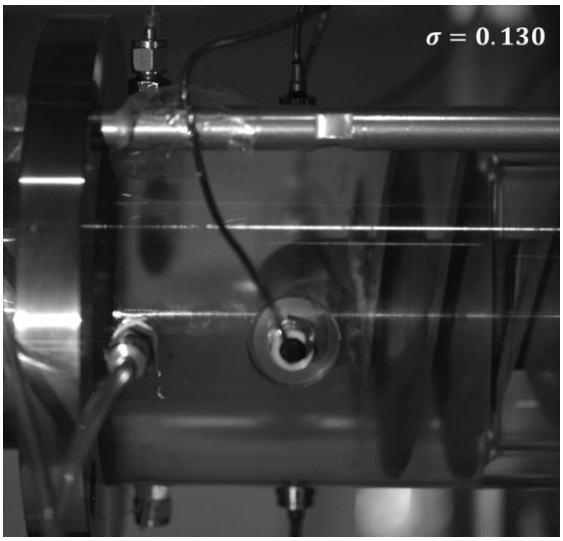

Figure 10. High-speed visualization of the cavity at $\sigma = 0.130$

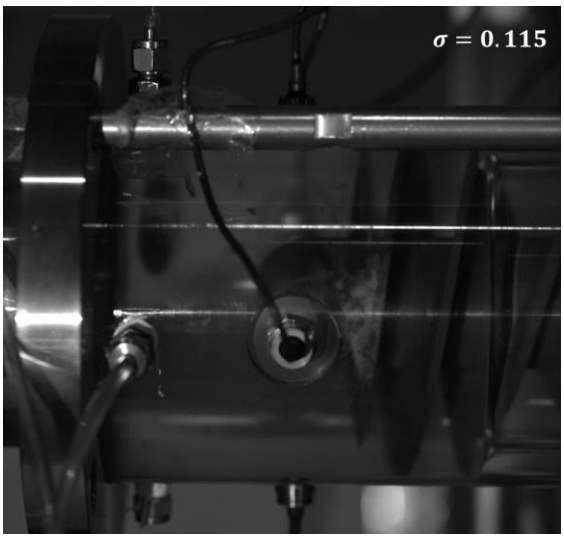

Figure 11. High-speed visualization of the cavity at $\sigma = 0.115$

The existence of the critical cavity length which enables the cavity to interact with the following blade leading edge can also be confirmed with early stages of the cavity development. At $\sigma = 0.115$ and 0.130, normalized cavity length (see Figure 12) is less than 0.5 and the cavity is developed in the form of equal cavity length (same cavity is developed at both blades). Figures 10 and 11 show the visualization of the cavity in both cases. From the figures, it can be seen that the cavities are not enough to reach the following blade leading edge and no impact is exerted on the incidence angle. With respect to the following blade, those cavities are the same with non-cavitating condition.

Fig. 12 summarize the experiment results under various cavitation numbers. The abscissa is the cavitation number which is defined as follows:

$$\sigma = \frac{p_{inlet} - p_v}{\frac{1}{2}\rho U^2}. \quad (1)$$

If the cavitation number decreases, the difference between the inlet pressure and the vapor pressure decreases, and the system becomes more susceptible to cavitation. The ordinate is the normalized cavity length, which is the length of the TLVC normalized by the inducer throat chord length as shown in the right inset of Fig. 12. As the cavitation number gets lower than 0.11, the cavity length graph bifurcates and shows maximum difference at around $\sigma = 0.08$. This represents the alternate blade cavitation region where the two blades have different cavity lengths. The longer cavity length is represented with red line and the shorter one is with the blue line. Fig. 12 shows that, after the alternate blade cavitation onset, the magnitude (or the difference between two cavity

lengths) increases until certain cavitation number and then again decreases.

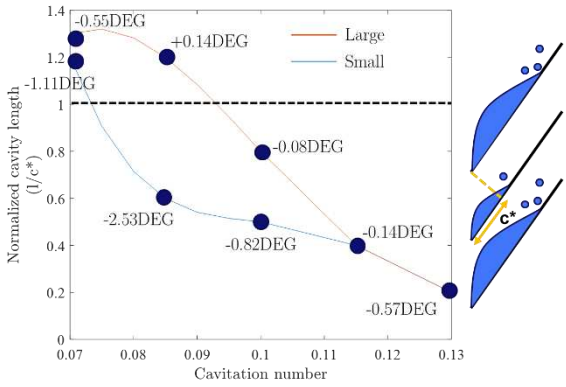

Figure 12. Cavity length and change in angle of attack under various cavitation number

Also shown in Fig. 12 as dark blue dots and captions are $\Delta\alpha$s at the given cavitation number and blade. Firstly, it can be seen in Figs. 8 and 9 that the alternate blade cavitation occurs due to uneven incidence for each blade. While the cavity on the red branch is large enough to interact with the leading edge of the following blade, it induces strong axial flow and, therefore, decreases the incidence angle of the following blade. Thus, the blade loading of the following blade, which is denoted as the blue branch, decreases and TLVC extent also decreases. Furthermore, by comparing the measured $\Delta\alpha$s at various cavitation number, changing magnitude of the alternate blade cavitation (whose trend is also observed by Huang et al. [9]) can be explained.

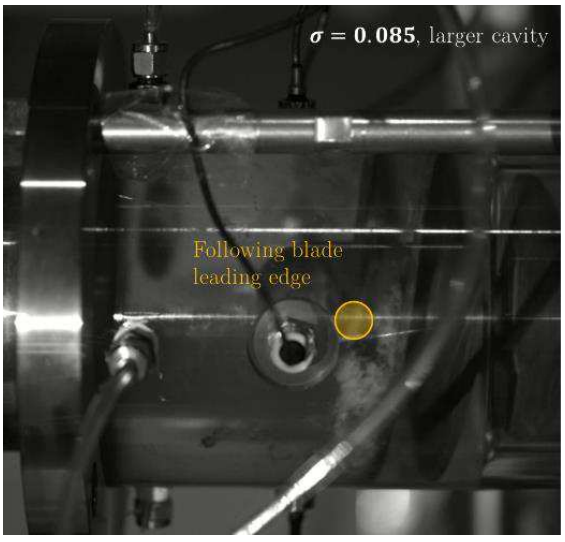

Figure 13. Visualization of the cavity at $\sigma = 0.085$

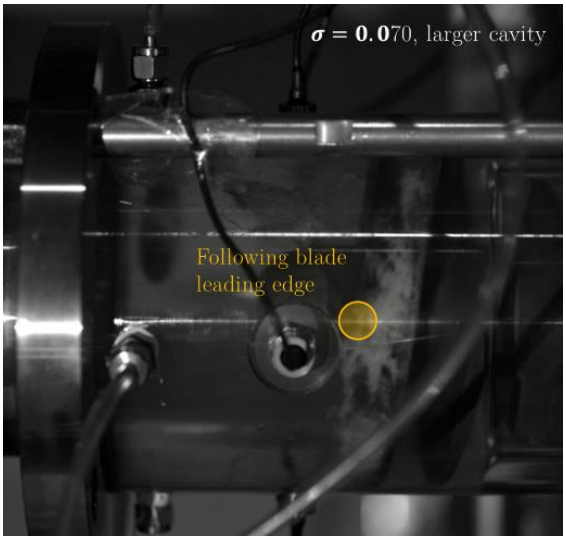

Figure 14. Visualization of the cavity at $\sigma = 0.070$

The magnitude of the alternate blade cavitation is the largest when the normalized length of the larger cavity is around 1. Before and after that point, decrease in angle of attack due to the larger cavity (which is $\Delta\alpha$ denoted on the blue branch) becomes smaller. Hence, it can be said that the magnitude of $\Delta\alpha$ is maximized when the normalized cavity length is near 1 ($l \approx c^*$). As the cavitation number decreases, the cavity length will increase, and the resulting magnitude of $\Delta\alpha$ and alternate blade cavitation increases until the cavity length reaches c*. After that, $\Delta\alpha$, and the alternate blade cavitation, will decrease.

Physically, maximized $\Delta\alpha$ at $l \approx c^*$ can be explained by the position of cavity collapse. While the collapse of the cavity bubble at the TLVC trailing edge induces large axial flow and decreases the incidence of the following blade, the position of the TLVC trailing edge plays a key role as proposed by Kang et al. [6]. Therefore, if the position of the cavity collapse coincides with the leading edge of the following blade, $\Delta\alpha$ is maximized and the alternate blade cavitation becomes the strongest. This can be more clearly seen in the Figures 13 and 14. Fig. 13 shows the larger cavity at $\sigma = 0.085$, and Fig. 14 shows larger cavity at $\sigma = 0.070$. At $\sigma = 0.085$, most of the cavities collapse near the leading edge of the following blade. However, at $\sigma = 0.070$, TLVC further extends until l/c*=1.3 and much less cavities collapse near the leading edge of the following blade. This reduces the induced axial flow and, accordingly, the incidence angle of the following blade less decreased.

4. SUMMARY AND CONCLUSIONS

In this study, the interaction between cavity and the following blade is experimentally investigated and quantified using particle image velocimetry and high-speed visualization of cavity. It was shown that

the collapse of the TLVC decreases the incidence of the following blade and, therefore, decreases its TLVC extent. Due to this interaction, alternate blade cavitation occurs. Also, the observed trend of alternate blade cavitation magnitude is explained by $\Delta\alpha$s at various cavitation number. It can be seen that the cavity-blade interaction is maximized when the normalized cavity length is around 1 and cavity collapses near the following blade leading edge, also when the alternate blade cavitation is the strongest.

ACKNOWLEDGEMENTS

This work was supported by BK21+ Program and Seoul National University Institute of Advanced Machines and Design (SNU-IAMD).

REFERENCES

[1] Tsujimoto, Y., Yoshida, Y., Maekawa, Y., Watanabe, S., and Hashimoto, T., 1997, "Observations of Oscillating Cavitation of an Inducer", *ASME J Fluids Engineering*, Vol. 119, pp. 775-781.

[2] Cervone, A., Bramanti, C., Rapposelli, E., Torre, L., and d'Agostino, L., 2006, "Experimental Characterization of Cavitation Instabilities in a Two-Bladed Axial Inducer", *AIAA J Propulsion and Power*, Vol. 22, pp. 1389-1395.

[3] Tsujimoto, Y., Kamijo, K., and Yoshida, Y., 1993, "A Theoretical Analysis of Rotating Cavitation in Inducers", *ASME J Fluids Engineering*, Vol. 115, pp. 135-141.

[4] Watanabe, S., Sato, K., Tsujimoto, Y., and Kamijo, K., 1999, "Analysis of Rotating Cavitation in a Finite Pitch Cascade Using a Closed Cavity Model and a Singularity Method", *ASME J Fluids Engineering*, Vol. 121, pp. 834-840.

[5] Horiguchi, H., Watanabe, S., and Tsujimoto, Y., 2000, "A Linear Stability Analysis of Cavitation in a Finite Blade Count Impeller", *ASME J Fluids Engineering*, Vol. 122, pp. 798-805.

[6] Kang, D., Yonezawa, K., Horiguchi, H., Kawata, Y., and Tsujimoto, Y., 2009, "Cause of Caviation Instabilities in Three Dimensional Inducer", *Int J Fluid Machinery and Systems*, Vol. 2, pp. 206-214.

[7] Kim, J., and Song, S. J., 2019, "Visualization of Rotating Cavitation Oscillation Mechanism in a Turbopump Inducer", *ASME J Fluids Engineering,* Vol. 141, pp. 091103.

[8] Yoon, Y., Kim, J., and Song, S. J., 2022, "Identification of Inducer Cavitation Instabilities Using High-Speed Visualization", *Experimental Thermal and Fluid Science*, Vol. 132, pp. 110548.

[9] Huang, J.-D., Aoki, M., and Zhang, J.-T., "Alternate Blade Cavitation on Inducer", *JSME International J Series B Fluids and Thermal Engineering,* Vol. 41, pp. 1-6.